Observation of intermolecular double-quantum coherence signal dips in nuclear magnetic resonance*

Shen Gui-Ping(沈桂平), Cai Cong-Bo(蔡聪波), Cai Shu-Hui(蔡淑惠)†, and Chen Zhong(陈 忠)

Department of Electronic Science and Communications Engineering, Fujian Key Laboratory of Plasma and Magnetic Resonance, State Key Laboratory of Physical Chemistry of Solid Surfaces, Xiamen University, Xiamen 361005, *China*

(Received 26 January 2011; revised manuscript received 6 April 2011)

The correlated spectroscopy revamped by asymmetric Z-gradient echo detection (CRAZED) sequence is modified to investigate intermolecular double-quantum coherence nuclear magnetic resonance signal dips in highly polarized spin systems. It is found that the occurrence of intermolecular double-quantum coherence signal dips is related to sample geometry, field inhomogeneity and dipolar correlation distance. If the field inhomogeneity is refocused, the signal dip occurs at a fixed position whenever the dipolar correlation distance approaches the sample dimension. However, the position is shifted when the field inhomogeneity exists. Experiments and simulations are performed to validate our theoretic analysis. These signal features may offer a unique way to investigate porous structures and may find applications in biomedicine and material science.

Keywords: nuclear magnetic resonance, distant dipolar field, intermolecular double-quantum coherence, signal dip

PACS: 33.25.+k, 31.30.jp, 34.80.Pa **DOI:** 10.1088/1674-1056/20/10/103301

1. Introduction

Intermolecular multiple-quantum coherence (iMQC) is an interesting phenomenon in highly polarized systems.[1] It originates from distant dipolar interactions between spins in different molecules and exhibits unusual properties.[2,3] The iMQC has been found to have applications in magnetic resonance imaging (MRI),[4−7] functional MRI,[6,8,9] and high-resolution nuclear magnetic resonance (NMR) spectroscopy.[10−13] The iMQC-based NMR has been proved to be structure-sensitive and widely used in non-invasive microstructure probing.[14−18]

During the exploration of structured samples, Richter *et al.*[19] first utilized the distant dipolar field (DDF) effect to investigate the structures of heterogeneous systems. Maraviglia and co-workers observed particular and unpredicted signal dips in multiple spin echoes experiments of porous media.[14,20,21] These signal dips occurred when the dipolar correlation distance became comparable to the average pore size of a porous system. They explained this phenomenon according to the role of internal field gradients associated with the sensitivity of magnetic susceptibility to local variations in solid-liquid porous interfaces. In their analysis[14,20,21] the influence of background inhomogeneous fields during the evolution period was not taken into account and no phase cycling was used. A similar phenomenon was observed by Bouchard *et al.*[22] The depth of the signal dip depended strongly on the orientation of sample with respect to the direction of static magnetic field. They attributed the observed single broad dip to the complex effects of gradient strength and direction, spin evolution time and sample orientation. They also believed that the internal magnetic field gradients generated from the interface of two phases offered the possibility to further characterize the sample geometry. However, Robyr and Bowtell[23] suggested that the absence of signal dips in the original multiple spin echoes experiments with structured samples might be due to the insufficient sampling of different dipolar correlation distances. The narrow signal dips observed by Capuani *et al.*[21] appeared to have been adequately sampled. All these investigations suggest that with the utilization of dipolar field effect, the structures of samples can be probed by varying the dipolar correlation dis-

*Project supported by the National Natural Science Foundation of China (Grant Nos. 10875101 and 11074209) and the Research Fund for the Doctoral Program of Higher Education of China (Grant No. 20090121110030).

†Corresponding author. E-mail: shcai@xmu.edu.cn

© 2011 Chinese Physical Society and IOP Publishing Ltd

tance. However, the dipolar field experienced by a spin at a specific position depends on all other spins surrounding it. This means that the DDF is generally non-local, (especially in the case of small gradient field),[24,25] which is difficult to obtain the analytical expression. In such a case, simulation plays an important role in obtaining the numerical solution.[26]

To further understand the physical source of iMQC signal dips, NMR spectroscopy and MRI are employed to study the variation of intermolecular double-quantum coherence (iDQC) signal intensity with sample geometry and background inhomogeneous field. Experimental and simulation results show that signal dips are correlated with the spatial modulation of DDF arising from the complex effect of coherence selection gradients (CSGs), sample geometry and inhomogeneous field. When the effect of field inhomogeneity is eliminated, signal dips occur whenever the dipolar correlation distance becomes comparable to the sample size.

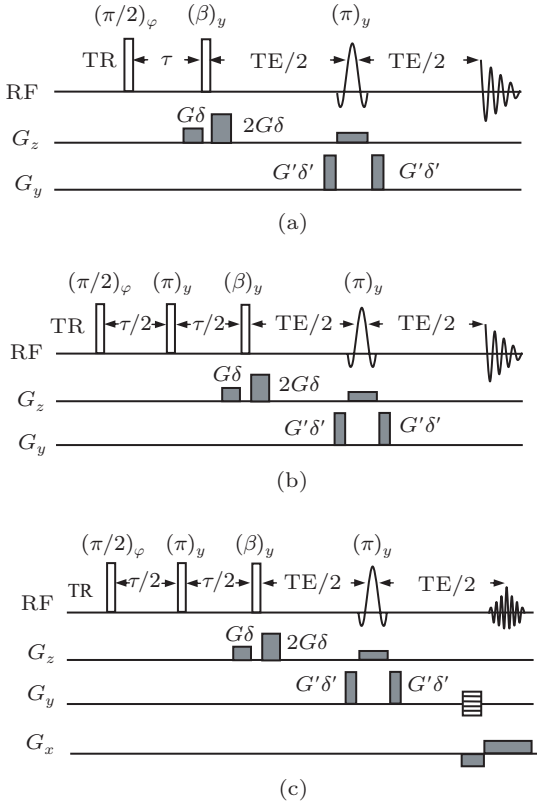


Fig. 1. Modified CRAZED pulse sequences for iDQC NMR and MRI studies. Panel (a) shows the sequence for spectroscopic study, with the influence of field inhomogeneity retained, defined as scheme $1^{\#}$; panel (b) exhibits the sequence for spectroscopic study, with the field inhomogeneity refocused by the π pulse in the middle of the evolution period, defined as scheme $2^{\#}$; and panel (c) indicates the sequence corresponding to panel (b) for MRI study.

2. Theoretical formalism

The pulse sequences are shown in Fig. 1, which are modified from the correlated spectroscopy revamped with asymmetric Z-gradient echo detection (CRAZED) sequence. Figures 1(a) and 1(b) are for spectroscopic study, and Fig. 1(c) is for MR imaging study. The influence of magnetic field inhomogeneity in the evolution period is retained in Fig. 1(a) (defined as scheme $1^{\#}$), while it is eliminated in Fig. 1(b) (defined as scheme $2^{\#}$) and Fig. 1(c) since there is an additional nonselective π refocusing pulse in the middle of the evolution period τ to refocus the dephasing of the magnetization due to magnetic field inhomogeneities. MR imaging is realized by adding a slice-selective π refocusing pulse and standard spin-warp imaging gradients to the spectroscopic sequences. All the RF pulses are not selective and applied along the y axis in the rotating frame and all the CSGs are applied along the z direction.

Consider an isolated spin-1/2 system (I spin system). For simplicity, the effects of radiation damping, diffusion and relaxation are neglected. Initially the net sample magnetization is aligned along the z direction, in line with the direction of external static magnetic field $\boldsymbol{B}_0$. During the application of the modified sequence shown in Fig. 1(a) or 1(b), the DDF $\boldsymbol{B}_{\rm d}$ generated by the spatially modulated magnetization refocuses a fraction of the magnetization, thus producing the signal. In the rotating frame, the Bloch equation including the DDF term can be expressed as

$$\frac{{\rm d}\boldsymbol{M}(\boldsymbol{r},t)}{{\rm d}t} = \gamma \boldsymbol{M}(\boldsymbol{r},t) \times \Big\{ \Big[\frac{\Delta\omega}{\gamma}\hat{\boldsymbol{z}} + \boldsymbol{G}(\boldsymbol{r})(\boldsymbol{r}\cdot\hat{\boldsymbol{s}}) \Big] + \boldsymbol{B}_{\rm d}(\boldsymbol{r},t) + \Delta\boldsymbol{B}(\boldsymbol{r},t) \Big\}, \quad (1)$$

where γ is the gyromagnetic ratio of the investigated nuclei; $\hat{\boldsymbol{z}}$ is the unit vector along the z direction; $\hat{\boldsymbol{s}}$ is the unit vector along the direction of CSGs; $\boldsymbol{M}(\boldsymbol{r},t)$ is the magnetization vector at position $\boldsymbol{r}$ at time t, $\boldsymbol{G}(\boldsymbol{r})$ is the first CSG vector along the $\hat{\boldsymbol{s}}$ direction at position $\boldsymbol{r}$; $\Delta\omega$ is the frequency offset of spin I, ($\Delta\omega = 0$ when the spin is in resonance) and $\Delta\boldsymbol{B}(\boldsymbol{r},t)$ represents the field inhomogeneity at position $\boldsymbol{r}$ at time t. The DDF is expressed as

$$\boldsymbol{B}_{\rm d}(\boldsymbol{r},t) = \frac{\mu_0}{4\pi}\int {\rm d}^3\boldsymbol{r}' \frac{1-3\cos^2\theta_{rr'}}{2\left|\boldsymbol{r}-\boldsymbol{r}'\right|^3} \times \left[3M_z(\boldsymbol{r}',t)\,\hat{\boldsymbol{z}} - \boldsymbol{M}(\boldsymbol{r}',t)\right], \quad (2)$$

where $\theta_{rr'}$ is the angle between the interspin vector $\boldsymbol{r}-\boldsymbol{r}'$ and the static magnetic field $\boldsymbol{B}_0$, μ_0 is

the vacuum magnetic permeability and $\boldsymbol{M}_z(\boldsymbol{r}', t)$ is the longitudinal magnetization component at position $\boldsymbol{r}'$. Generally, this dipolar field is non-local and depends strongly on the shape of sample. However, this equation has the form of a convolution integral and the DDF becomes local in k-space following a spatial Fourier transform. Therefore, equation (2) can be simplified in the k-space into

$$\boldsymbol{B}_{\rm d}(\boldsymbol{k}, t) = \frac{\mu_0}{6}\left[3(\hat{\boldsymbol{k}}\cdot\hat{\boldsymbol{z}})^2 - 1\right] \times \left[3M_z(\boldsymbol{k}, t)\hat{\boldsymbol{z}} - \boldsymbol{M}(\boldsymbol{k}, t)\right], \quad (3)$$

where

$$\boldsymbol{M}(\boldsymbol{k}, t) = \int_{-\infty}^{+\infty} {\rm d}^3\boldsymbol{r} \exp(-{\rm i}\,\boldsymbol{k}\cdot\boldsymbol{r})\boldsymbol{M}(\boldsymbol{r}, t) \quad (4)$$

and $\hat{\boldsymbol{k}} = \boldsymbol{k}/k$ and $k = \gamma G\delta$. The direction of $\boldsymbol{k}$ is specified by the CSG direction. For a uniform cylindrical sample, the evolution of magnetization can be found by solving Eqs. (1) and (2). The transverse magnetizations created from the pulse sequences shown in Figs. 1(a) and 1(b) are respectively given by[27−29]

$$M_+(\boldsymbol{r}, t_2) = \frac{M_0}{2}\left\{\begin{array}{l}\left[{\rm e}^{{\rm i}[(\Delta\omega+\gamma\Delta B(\boldsymbol{r}))\tau+\boldsymbol{k}\cdot\boldsymbol{r}]} - {\rm e}^{-{\rm i}[(\Delta\omega+\gamma\Delta B(\boldsymbol{r}))\tau+\boldsymbol{k}\cdot\boldsymbol{r}]}\right] \\ -\cos\beta\left[{\rm e}^{{\rm i}[(\Delta\omega+\gamma\Delta B(\boldsymbol{r}))\tau+\boldsymbol{k}\cdot\boldsymbol{r}]} + {\rm e}^{-{\rm i}[(\Delta\omega+\gamma\Delta B(\boldsymbol{r}))\tau+\boldsymbol{k}\cdot\boldsymbol{r}]}\right]\end{array}\right\} \times {\rm e}^{-{\rm i}[2\boldsymbol{k}\cdot\boldsymbol{r}+\gamma B_{\rm d}(\boldsymbol{r},\boldsymbol{t})(TE+t_2)]}\,{\rm e}^{{\rm i}(\Delta\omega+\gamma\Delta B(\boldsymbol{r}))t_2}, \quad (5a)$$

and

$$M_+(\boldsymbol{r}, t_2) = \frac{M_0}{2}\left[\left({\rm e}^{{\rm i}\,\boldsymbol{k}\cdot\boldsymbol{r}} - {\rm e}^{-{\rm i}\,\boldsymbol{k}\cdot\boldsymbol{r}}\right) - \cos\beta\left({\rm e}^{{\rm i}\,\boldsymbol{k}\cdot\boldsymbol{r}} + {\rm e}^{-{\rm i}\,\boldsymbol{k}\cdot\boldsymbol{r}}\right)\right]{\rm e}^{-{\rm i}[2\boldsymbol{k}\cdot\boldsymbol{r}+\gamma B_{\rm d}(\boldsymbol{r},t)(TE+t_2)]}\,{\rm e}^{{\rm i}(\Delta\omega+\gamma\Delta B(\boldsymbol{r}))t_2}. \quad (5b)$$

The relevant longitudinal magnetizations are

$$M_z(\boldsymbol{r}) = -M_0\frac{\sin\beta}{2}\left\{{\rm e}^{{\rm i}[(\Delta\omega+\gamma\Delta B(\boldsymbol{r}))\tau+\boldsymbol{k}\cdot\boldsymbol{r}]} + {\rm e}^{-{\rm i}[(\Delta\omega+\gamma\Delta B(\boldsymbol{r}))\tau+\boldsymbol{k}\cdot\boldsymbol{r}]}\right\}, \quad (6a)$$

and

$$M_z(\boldsymbol{r}) = -M_0\frac{\sin\beta}{2}\left({\rm e}^{{\rm i}\,\boldsymbol{k}\cdot\boldsymbol{r}} + {\rm e}^{-{\rm i}\,\boldsymbol{k}\cdot\boldsymbol{r}}\right), \quad (6b)$$

where M_0 is the equilibrium magnetization of spin I and β is the flip angle of the second RF pulse. In Eqs. (5b) and (6b) the dephasing of magnetization due to magnetic field inhomogeneity in the evolution period τ is eliminated by the π refocusing pulse.

When the strength of CSG is strong enough (i.e. $\gamma G\delta \gg 2\pi/L$, where L is the sample dimension), the DDF can also be reduced into a localized one with a magnitude proportional to the longitudinal magnetization. The observed signal can be obtained by integrating the transverse magnetization over the entire sample. The iDQC signal obtained from Eqs. (5a) and (5b) are

$$M_+^{\rm iDQC}(t_2) = M_0\sin^2\frac{\beta}{2}\{{\rm J}_1(\xi) - {\rm J}_3(\xi)\} \times {\rm e}^{{\rm i}(2\Delta\omega+\gamma\Delta B)\tau}\,{\rm e}^{{\rm i}(\Delta\omega+\gamma\Delta B)t_2}, \quad (7a)$$

and

$$M_+^{\rm iDQC}(t_2) = M_0\sin^2\frac{\beta}{2}\{{\rm J}_1(\xi) - {\rm J}_3(\xi)\} \times {\rm e}^{{\rm i}(\Delta\omega+\gamma\Delta B)t_2}, \quad (7b)$$

where $\xi = -\gamma\mu_0 M_0\sin\beta(t_2 + TE)$, ${\rm J}_1(\xi)$ and ${\rm J}_3(\xi)$ are the 1st and 3rd order Bessel functions, respectively, and the optimal value for β is $2\pi/3$.[30]

3. Materials and methods

All experiments were performed at 298 K on a Varian 7.0 T/160 mm research MRI scanner system with a 63/95 mm quad birdcage coil. The CSGs were applied with a duration of 1.2 ms and variable strengths. A pair of spoiled gradients were applied with strength $G' = 0.1$ T/m and duration $\delta' = 1$ ms. The RF pulse flip angle β was $2\pi/3$. A four-step phase-cycling was used to select pure iDQC signal and suppress conventional single-quantum coherence (SQC) and other undesired signals from unexpected coherence transfer pathways. The phases for the first RF pulse and the receiver were (x, $-x$, y, $-y$) and (x, x, $-x$, $-x$), respectively.[28]

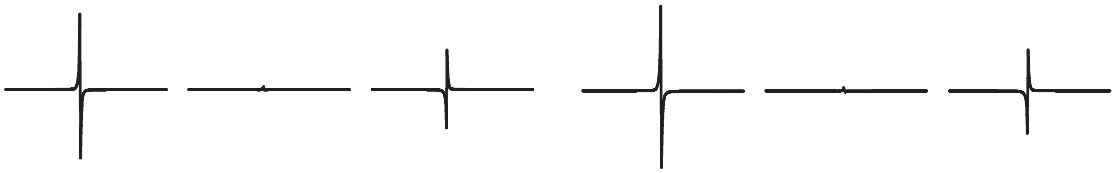
A series of cylindrical plastic tubes with outer diameters of 0.25, 0.50, 1.0, 2.0, 3.0 cm (the corresponding inner diameters were 0.20, 0.43, 0.90, 1.84, and 2.80 cm) filled with water mildly doped with 0.1% $CuSO_4$ were prepared for quantitatively studying the properties of iDQC signal dips. The transverse relaxation time T_2 of the sample measured with CMPG-T_2

sequence was 0.80 s. The actual residual field inhomogeneity ΔB was calculated according to the formula $\Delta B = \left(\pi\Delta\upsilon_{1/2} - 1/T_2\right)/\gamma$, where $\Delta\upsilon_{1/2}$ is the half-height linewidth of a resonance. For the cylindrical samples, the field inhomogeneities were set to be 5, 30, 50, and 100 Hz, respectively, by adjusting the electric currents of shim coils. The $\pi/2$ RF pulse width was 36 μs. To demonstrate that the observed signals were really from iDQCs, magic angle gradient experiments were carried out by using the pulse sequences shown in Figs. 1(a) and 1(b), respectively. The strength of CSG was $G = 0.1 \times 10^{-2}$ T/m and the 4-step phase cycling scheme was applied.

To further understand experimental results, computer simulations were performed. The DDF was first computed directly in the k-space from Eq. (3) with a fifth-order Cash–Karp Runge–Kutta formalism.[26,31] The result was then used to calculate the DDF in real space and magnetization based on Eqs. (1) and (2), respectively, which were used to calculate the DDF in the k-space again. This iterative process was repeated from $t = 0$ to t_{final}. The sample was an homogeneous spin system in a cylinder with a diameter of 3.75 mm and a height of 38.75 mm, which was embedded in the middle of a cuboid with a size of 5 mm×5 mm×40 mm. The cuboid was represented by evenly distributed grid points ($64 \times 64 \times 512$ points and the distance between two adjacent points was 78.125 μm). The physical parameters for the spin system were as follows: magnetization density $M_0 = 0.023$ A/m ($M_0 = 0$ outside the cylinder), $T_1 = 1$ s, $T_2 = 0.2$ s, diffusion coefficient $D_T = 3.0 \times 10^{-9}$ m/s^2, and frequency offset $\Delta\omega = 0$. The pulse sequence used in simulation was the modified CRAZED sequence in Fig. 1(b). The parameters for the sequence were as follows: $\tau = 10$ ms, $TE = 50$ ms, the CSGs were applied along the z direction with a duration of $\delta = 1.2$ ms and variable strength G to obtain different values of dipolar correlation distance d_{c}. The simulation program was written in Matlab 7.0 (Mathworks, MA, USA).

4. Results and discussion

The one-dimensional (1D) NMR spectra from the cylindrical water sample with 1.0 cm outer diameter using the pulse sequences shown in Figs. 1(a) and 1(b) are presented in Fig. 2. It shows that the signal intensities acquired with the CSGs along the z direction are about twice as strong as those acquired with the CSGs along the x direction, but they are close to zero when the CSGs are along the magic angle direction. This indicates that the signals really come from iDQCs, no matter whether the effect of field inhomogeneity is eliminated, as expected theoretically.



(a) (b)

Fig. 2. The 1D NMR spectra from a cylindrical water sample with 1.0 cm outer diameter. Panel (a) indicates signals from the pulse sequence shown in Fig. 1(a) with the CSGs along the z direction (left), the magic angle direction (middle) and the x direction (right); and panel (b) exhibits signals corresponding to those in panel (a), from the pulse sequence shown in Fig. 1(b).

To study iDQC signal dips, a series of one-dimensional (1D) ^{1}H iDQC spectra of water in an NMR tube of 1.0 cm in outer diameter were acquired with different strengths of CSGs. All experimental parameters were set to be the same except for the G values. The pulse sequence shown in Figs. 1(a) and 1(b) were used. The plots of relative signal intensity versus k ($k = \gamma G\delta$) are given in Fig. 3. For comparison, all the signal intensities are relative to the first data point which is normalized. The field inhomogeneities are 5, 30, 50, and 100 Hz, respectively. There are signal dips no matter whether the influence of field inhomogeneity is included. When the influence of field inhomogeneity is included, the positions of the dips shift with the variation of field inhomogeneity.[32] The greater the field inhomogeneity, the larger the absolute k value is. The signal dips appear pairwise at both positive and negative k values. Furthermore, the degree of signal dips decreases (i.e. larger signal intensity remains) with the increase of field inhomogeneity. When

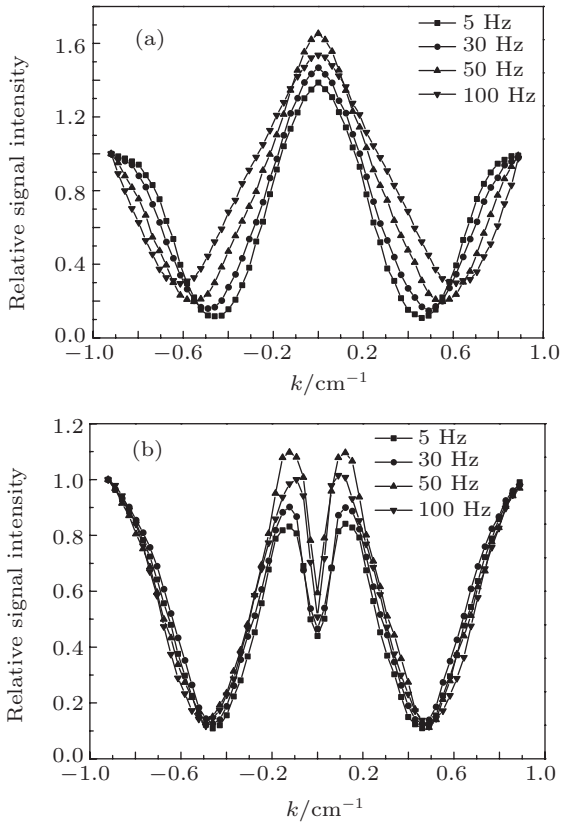


Fig. 3. Variations of iDQC signal intensity of water in a 1.0-cm cylindrical tube versus k ($k = \gamma G\delta$). The field inhomogeneities were 5, 30, 50 and 100 Hz, respectively. Panel (a) shows the case where the pulse sequence shown in Fig. 1(a) is used; and panel (b) indicates the case where the pulse sequence shown in Fig. 1(b) is used.

the influence of field inhomogeneity is eliminated, the signal dips still exist (Fig. 3(b)), which is different from previous observation.[22] In such a case, the dips appear at almost the same positions under different inhomogeneous field conditions. As shown in Fig. 3(a), when the influence of inhomogeneous field is included, a strongest iDQC signal is obtained at $k = 0$ (i.e. in the absence of CSGs). On the contrary, the signal intensity decreases when the inhomogeneous field is eliminated at $k = 0$ (Fig. 3(b)). These results demonstrate that the background inhomogeneous field plays an important role in generating DDF in the absence of CSGs. When the influence of field inhomogeneity is eliminated by the π refocusing pulse, the DDF can be restored only by the effect of sample geometry at $k = 0$. Therefore, the DDF becomes very weak and the signals decay quickly (Fig. 3(b)). On the other hand, larger field inhomogeneity causes faster signal attenuation. Thus the signal enhancement effect is reduced when the field inhomogeneity reaches a certain extent (compare the results for $\Delta B = 100$ Hz and 50 Hz around $k = 0$ in Fig. 3(a)). The order of signal intensities around $k = 0$ in Fig. 3(b) may follow the same reason. Since the π refocusing pulse may be imperfect in practical experiments, the influence of inhomogeneous field cannot be completely eliminated. Therefore, the signal is affected by the residual field inhomogeneity at weak CSGs.

As the signal dips are located at both positive and negative k positions symmetrically, to simplify the analysis, we consider only the positive case. The positive positions of signal dips for the samples in different cylindrical tubes are summarized in Table 1. In previous studies, the occurrence of signal dips was considered as an effect related to dipolar correlation distance.[20,21] It was suggested that when the dipolar correlation distance was comparable to the average length-scale of sample heterogeneity, a signal cancellation would occur. Our observation is consistent with these studies. As shown in Table 1 when the field inhomogeneity is eliminated, the values of dipolar correlation distance d_c ($d_c = \pi/\gamma G\delta$) are about (0.21 ± 0.01), (0.46 ± 0.02), (0.99 ± 0.02), (2.06 ± 0.02), and (3.17 ± 0.01) cm close to the inner diameters of sample tubes 0.20, 0.43, 0.90, 1.84, and 2.80 cm, respectively.

The question is how the dipolar correlation distance and sample geometry take effect on the iDQC signal amplitude and cause the signal dips. Consider an infinitely long cylindrical sample with a diameter of D. When the influence of field inhomogeneity is eliminated, the magnetization is spatially modulated only by the external pulse field gradient G with duration δ in the z direction. Simulations were performed in this case. The simulation results are shown in Fig. 4. The variations of DDF intensity along the z direction under different dipolar correlation distances (i.e. different CSGs) are shown in Fig. 4(a). When the dipolar correlation distance is set to be the sample diameter (i.e. $d_c = D$), the DDF amplitude reaches a minimum. The DDF amplitude increases when d_c deviates from D. This indicates that the refocusing effect of DDF on the magnetization would be is minimized in the case of $d_c = D$. As a consequence, the iDQC signal intensity becomes weakest and a signal dip appears when $d_c = D$. This is verified by the variations of iDQC signal intensity profiles shown in Fig. 4(b).

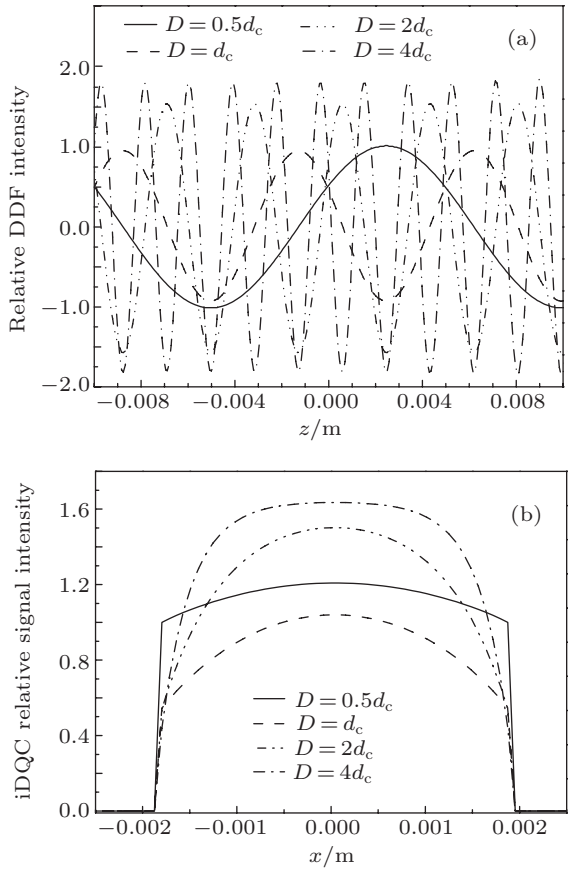


Fig. 4. Simulation results of the variations of DDF and iDQC signal intensities in a cylindrical tube along the z direction and in the xy plane under different dipolar correlation distances. Panel (a) shows the variations of DDF intensity along the z direction; and panel (b) exhibits the variations of iDQC signal intensity profile along the x direction.

When the influence of inhomogeneous field cannot be neglected, i.e, an internal magnetic field gradient G_{internal} exists in the sample, the coherence between spins due to the external CSG G is destroyed. Moreover, the field inhomogeneity may cause additional spatial modulation of the transverse magnetization. In such a case, the magnetization is spatially modulated by the effective magnetic field gradient which can be expressed as $G_{\text{eff}} = G + G_{\text{internal}}$. The magnetization would then form a complex spatial helix. When G_{internal} value is much smaller than G, it can be neglected and $G_{\text{eff}} \approx G$. In other words, the signal dips are hardly affected by the inhomogeneous field. However, with the increase of inhomogeneous field, G_{internal} value increases too. To overcome the additional spatial modulation of transverse magnetization caused by G_{internal} and make the modulation effect the same as the case of $d_c = D$, the strength of external gradient G must be varied consequently. The greater the G_{internal}, the greater the G must be. Consequently, the positions of signal dips deviate from $k = \gamma G\delta$ and shift toward larger k values with the increase of G_{internal}. Furthermore, the signal intensity increases slightly at the positions of signal dips with the increase of G_{internal}. This may be because the larger G_{internal} value corresponds to the larger G value (i.e. the larger DDF) at the positions of signal dips. Accordingly, the degree of signal dip becomes weaker under larger inhomogeneous field. This is what we see in Fig. 3 and Table 1.

Table 1. Positive positions of the signal dips observed with different cylindrical tubes under different inhomogeneous fields.

Inner diameter of sample tube/cm	Residual field inhomogeneity/Hz	k value at signal dip/cm^{-1}		Average d_c in scheme 2$^{\#}$ at a signal dip/cm
		Scheme 1$^{\#}$	Scheme 2$^{\#}$	
0.20	5	2.38	2.37	0.21 ± 0.01
	30	2.44	2.37	
	50	2.55	2.38	
	100	2.72	2.38	
0.43	5	1.11	1.09	0.46 ± 0.02
	30	1.16	1.09	
	50	1.23	1.09	
	100	1.33	1.10	
0.90	5	0.46	0.47	0.99 ± 0.02
	30	0.50	0.51	
	50	0.55	0.52	
	100	0.61	0.52	
1.84	5	0.24	0.24	2.06 ± 0.02
	30	0.27	0.24	
	50	0.31	0.24	
	100	0.39	0.25	
2.80	5	0.15	0.15	3.17 ± 0.01
	30	0.18	0.16	
	50	0.22	0.16	
	100	0.29	0.16	

The appearance of iDQC signal dips can be further verified in iDQC MRI as shown in Fig. 5. The sample was water in two cylindrical tubes with 0.25 cm and 3.0 cm in outer diameter (inner diameters are 0.20 cm and 2.80 cm, respectively). In Fig. 5(a), $k = 2.38$ cm^{-1} corresponds to a position of signal dip for the small tube (Table 1), therefore the signal intensity from the small tube approaches to a minimum, while the signal intensity from the large tube is not affected. In Fig. 5(b), $k = 0.16$ cm^{-1} corresponds to a position of signal dip for the large tube, so the result is contrary to the former. An iDQC image with $G = 0.04$ T/m is given in Fig. 5(c) for comparison. This CSG setting is not related to any signal dip. All the signal profiles are shown in Fig. 5(d). The signal intensity of water in the small tube at the signal dip is about 0.54 times that at $G = 0.04$ T/m, while for the large tube this ratio becomes about 0.42.

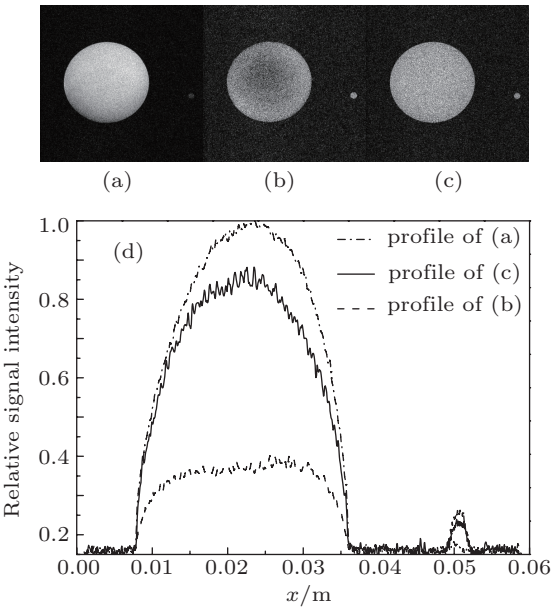


Fig. 5. Images and corresponding signal profiles of a 2-mm slice of water in two cylindrical tubes with 0.25 and 3.0 cm in outer diameter (0.20 cm and 2.80 cm inner diameter, respectively) obtained with different k values using the pulse sequence shown in Fig. 1(d), with $G = 0.47 \times 10^{-2}$ T/m and $k = 2.38$ cm^{-1} (a); $G = 0.3 \times 10^{-3}$ T/m and $k = 0.16$ cm^{-1} (b); $G = 0.04$ T/m and $k = 18.4$ cm^{-1} (c). Panel (d) shows profiles of panels (a)–(c). The field of view (FOV) = 60 mm × 60 mm and matrix size = 256 × 256.

5. Conclusion

The CRAZED sequence is modified to investigate the signal dip in iDQC NMR spectroscopy and MR imaging. The occurrence of signal dips is related to sample geometry, inhomogeneous field and CSGs. When the influence of field inhomogeneity is eliminated, the signal dips will stably appear at the position of $k = \gamma G\delta$ if the dipolar correlation distance is equal to the geometric size of the sample. This feature of iDQC signal may offer a unique way to investigate porous structure and may find applications in biomedicine and materials science.

References

[1] Warren W S, Richter W, Andreotti A H and Farmer II B T 1993 *Science* **262** 2005
[2] Zanker P P, Schmiedeskamp J, Spiess H W and Acosta R H 2008 *Phys. Rev. Lett.* **100** 213001
[3] Shen G P, Cai C B, Cai S H and Chen Z 2009 *Chin. Phys.* B **18** 4797
[4] Qian Y X, Zhao T, Hue Y K, Ibrahim T S and Boada F E 2010 *Magn. Reson. Med.* **63** 543
[5] Li J Q, Wang Y, Jiang Y, Xie H B and Li G Y 2009 *Magn. Reson. Imaging* **27** 988
[6] Branca R T, Chen Y M, Mouraviev V, Galiana G, Jenista E R, Kumar C, Leuschner C and Warren W S 2009 *Magn. Reson. Med.* **61** 937
[7] Tang X, Hong L M and Zu D L 2010 *Chin. Phys.* B **19** 078702
[8] Schneider J T and Faber C 2008 *Magn. Reson. Med.* **60** 850
[9] Liu Y, Li J Q and Li G Y 2008 *Magn. Reson. Mat. Phys. Biol. Med.* **21** 199
[10] Eliav U and Navon G 2008 *J. Magn. Reson.* **190** 149
[11] Fu R Q 2009 *Chem. Phys. Lett.* **483** 147
[12] Zhou X, Luo J, Sun X P, Zeng X Z, Ding S W, Liu M L and Zhan M S 2004 *Phys. Rev.* B **70** 052405
[13] Ren T T, Luo J, Sun X P and Zhan M S 2009 *Chin. Phys.* B **18** 4711
[14] Capuani S, Branca R T, Alesiani A and Maraviglia B 2003 *Magn. Reson. Imaging* **21** 413
[15] Cho J H, Ahn S, Lee C, Hong K S, Chung K C, Chang S K, Cheong C and Warren W S 2007 *Magn. Reson. Imaging* **25** 626
[16] Li Z F, Li W S, Li X J, Pei F K, Li Y X and Lei H 2007 *Magn. Reson. Imaging* **25** 412
[17] Zhou X, Sun X P, Luo J, Zhan M S and Liu M L 2009 *J. Magn. Reson.* **196** 200
[18] Zhang L P, Zheng Z, Liang J C, Le X Y, Zou C, Liu H L and Liu Y 2008 *Chin. Phys.* B **17** 4619
[19] Richter W, Lee S H, Warren W S and He Q H 1995 *Science* **267** 654
[20] Alessandri F M, Capuani S and Maraviglia B 2002 *J. Magn. Reson.* **156** 72
[21] Capuani S, Curzi F, Alessandri F M, Maraviglia B and Bifone A 2001 *Magn. Reson. Med.* **46** 683
[22] Bouchard L S, Wehrli F W, Chin C L and Warren W S 2005 *J. Magn. Reson.* **176** 27
[23] Robyr P and Bowtell R 1997 *J. Chem. Phys.* **106** 467
[24] Wong C K and Zhong J H 2009 *Concepts Magn. Reson.* Part A **34** 76
[25] Chen S, Zhu X Q, Cai S H and Chen Z 2008 *Chin. Phys.* B **17** 915

[26] Lin T, Sun H J, Chen Z, You R Y and Zhong J H 2007 *Magn. Reson. Imaging* **25** 1409

[27] Warren W S, Ahn S, Mescher M, Garwood M, Ugurbil K, Richter W, Rizi R R, Hopkins J and Leigh J S 1998 *Science* **281** 247

[28] Cai C B, Lin Y Q, Cai S H, Chen Z and Zhong J H 2008 *J. Magn. Reson.* **193** 94

[29] Huang Y Q, Zhang W, Cai S H, Zhong J H and Chen Z 2010 *Chem. Phys. Lett.* **492** 174

[30] Chen Z, Chen Z W and Zhong J H 2002 *J. Chem. Phys.* **117** 8426

[31] Enss T, Ahn S and Warren W S 1999 *Chem. Phys. Lett.* **305** 101

[32] Charles-Edwards G D, Payne G S, Leach M O and Bifone A 2004 *J. Magn. Reson.* **166** 215